Study on the synthesis, physicochemical, electrochemical properties, molecular structure and antifungal activities of the 4-pyrrolidinopyridine Mg(II) meso-tetratolylporphyrin complex

S. Jabli, S. Hrichi, R. Chaabane-Banaoues, F. Molton, F. Loiseau, Thierry Roisnel, I. Turowska-Tyrk, H. Babba, H. Nasri

Study on the Synthesis, Physicochemical, Electrochemical Properties, Molecular Structure and Antifungal Activities of the 4-Pyrrolidinopyridine Mg(II) *Meso*-tetratolylPorphyrin Complex

Souhir Jabli [a], Soukaina Hrichi [a], Raja Chaabane-Banaoues[b], Florian Molton [c], Frédérique Loiseau [c], Thierry Roisnel [d], Ilona Turowska-Tyrk [e], Hamouda Babba [b] Habib Nasri [a,]*

[a] : *University of Monastir, Laboratory of Physical Chemistry of Materials (LR01ES19), Faculty of Sciences of Monastir, Avenue de l'environnement, 5019 Monastir, Tunisia.*
[b:] *University of Monastir, Faculty of Pharmacy, Laboratory of Medical and Molecular Parasitology-Mycology (LP3M), LR12ES08, 5000 Monastir, Tunisia.*
[c]*: Département de Chimie Moléculaire, 301 rue de la Chimie, Université Grenoble Alpes, CS 40700, 38058 Grenoble, Cedex 9, France*
[d]*: Institute of Chemical Sciences of Rennes, UMR 6226, University of Rennes 1, Beaulieu Campus, 35042 Rennes, France*
[e]*: Faculty of Chemistry, Wroclaw University of Science and Technology, Wybrzeże Wyspiańskiego 27, 50-370 Wrocław, Poland.*

Abstract

A novel magnesium(II) metalloporphyrin namely the bis(4-pyrrolidinopyridine)[*meso*-tetra(*p*-tolyl)porphyrinato)]magnesium(II) dichloromethane desolate complex with the formula $[Mg(TTP)(4\text{-pypo})_2]\cdot CH_2Cl_2$ (**I**) has been synthetized and fully characterized by UV-Vis, fluorescence, IR, ^1H NMR spectroscopy and mass spectrometry. The X-ray molecular structure shows that **I** presents two molecules (1 and 2) $[Mg1(TTP)(4\text{-pypo})_2]$ and $[Mg2(TTP)(4\text{-pypo})_2]$ in the asymmetric unit while the Hirshfeld surface analysis on this hexacoordinated Mg(II) porphyrin species indicates that the crystal lattice is mainly sustained by C—H···C, C—H···Cg (Cg is the centroid of a phenyl ring) and C—H···Cl intermolecular interactions. The cyclic voltammetry data of **I** is also reported. The bioactivity of the H_2TTP, the [Mg(TTP)] starting material and $[Mg(TTP)(4\text{-pypo})_2]\cdot CH_2Cl_2$ (**I**) was evaluated *in vitro*, by examining their inhibitory effect against three strains of *Candida viz. C. albicans, C. glabrata* and *C. tropicalis* with MIC values in the range 2.5 to 10 $\mu g.mL^{-1}$. The screening of the susceptibility of *M. canis* and *T. rubrum* clinical strains on the three porphyrinic derivatives is also reported.

* Corresponding author. Fax: +216 73 500 278.
E-mail address: hnasri1@gmail.com and Habib.Nasri@fsm.rnu.tn (Habib Nasri).

Keywords: Magnesium(II) porphyrin complex; X-ray molecular structure; Photophysical properties; Cyclic voltammetry; Antifungal and Biological Activities.

1. Introduction

Divalent metals porphyrin complexes could be divided in two classes. The first one made by open-shell paramagnetic metal ions such as Mn(II), Fe(II) and Co(II) and the second class is made by diamagnetic metal ions such as Zn(II), Cd(II) and Mg(II). The first class of divalent metalloporphyrins were intensively studied because they are paramagnetic and have the ability to change their oxidation state. These porphyrin complexes were first used as models for hemoproteins and then in many other fields especially as catalysis **[1,2]**, chemical sensors, **[3,4]** semiconductors **[5]**, and in nonlinear optic devices **[6]**. The diamagnetic M(II) metalloporphyrins except those of Zn(II), which were very studied, Cd(II) and Mg(II) porphyrin complexes were much less investigated. Thus, Cambridge Structural Database (CSD Version 5.42, update of September 2021) **[7]** contains the molecular structures of 1461 Zn–porphyrin complexes and only 49 and 80 Cd and Mg metalloporphyrins, respectively. Notably, M(II) diamagnetic porphyrins provide simpler systems than those of Co(II) and Fe(II) or other d transition metals to evaluate the influence of axial ligands on the structural and photophysical properties of metalloporphyrins. Magnesium(II) metalloporphyrins were investigated first as models for chlorophyll in which the Mg(II) center metal is coordinated to a reduced porphyrin. Over the past decade, our research group reported several investigations concerning new magnesium *meso*-arylporphyrin coordination compounds **[8-13]**.

Invasive fungal infections are a growing threat with high morbidity and mortality. The discovery of new drug candidates against human pathogenic fungi has become a necessity for many researchers **[14]**. In recent years a great deal of research has been devoted to the preparation of entities capable of inhibiting the activities of fungi **[15-17]**. Notably, the past decade has witnessed intense research devoted to the antifungal activities of porphyrin species **[18-20]**.

In order to get more insight into the photophysical, electrochemical and structural properties of magnesium(II) metalloporphyrins as well as the antifungal performance of these coordination compounds, a new Mg(II) porphyrin derivative was prepared namely the bis(4-pyrrolidinopyridine)[*meso*-tetra(*p*-tolyl)porphyrinato)]magnesium(II) dichloromethane desolate complex with the formula $[Mg(TTP)(4\text{-pypo})_2]\cdot CH_2Cl_2$ (**I**).

2. Experimental Section

2.1. Materials and methods

IR and UV-vis spectroscopy: Solid IR spectra were obtained with a PerkinElmer Spectrum Two FTIR
spectrometer. The UV/Vis spectra were recorded with a WinASPECT PLUS (validation for SPECORD PLUS version 4.2) scanning spectrophotometer.

MS spectrometry: Electrospray (ESI) spectra were carried out using an amaZon speed ion trap instrument and the ESI-HRMS spectra were recorded in an using LTQ Orbitrap XL apparatus (Thermo Scientific) equipped with an electrospray ionization (ESI) source. Solutions in dichloromethane were used for the analysis.

Emission spectroscopy: The emission spectra were recorded at room temperature with a Horiba Scientific Fluoromax-4 spectrofluorometer. The luminescence lifetime measurements were performed for excitation at λ = 450 nm using the second harmonic of a titanium–sapphire laser (picosecond Tsunami laser spectra physics 3950-M1BB and 39868- 03 pulse picker doubler) at an 800 kHz repetition rate. Fluotime 200 from AMS technologies was used for the decay acquisition. It consists of a GaAs microchannel plate photomultiplier tube (Hamamatsu model R3809U-50) followed by a time-correlated single photon counting system from Picoquant (PicoHarp300). The ultimate time resolution of the system is close to 30 ps. The luminescence decays were analyzed with the FLUOFIT software available from Picoquant. The mission quantum yields were determined at room temperature in dichloromethane solutions by using the optically dilute method **[21]**. [Zn(TPP)] in air-equilibrated dichloromethane solution was used as a quantum yield standard (ϕ_f = 0.031) **[22]**.

Electrochemistry: Cyclic voltammetry (CV) experiments were performed with CH-660B potentiostat (CH Instruments). All analytical experiments were conducted at room temperature under an argon atmosphere (argon stream) in a standard one compartment, three-electrode electrochemical cell. Tetra-nbutylammonium perchlorate (TBAP) was used as a supporting electrolyte (0.2 M) in dichloromethane previously distilled over calcium hydride under argon. An automatic ohmic drop compensation procedure was systematically implemented before the CV data were recorded with electrolytic solutions containing the studied compounds at concentrations of ca. 10^{-3} M. CH Instruments vitreous carbon (ϕ = 3 mm) working electrodes were polished with 1 mm diamond paste before each recording. The $Ag/AgNO_3$ 0.01 M (TBAP 0.2 in CH_2Cl_2) redox couple was used as the reference electrode. The potential of the ferrocene/ferrocenium redox couple was used as an internal reference (86 mV vs. $Ag/AgNO_3$ under our experimental conditions). For comparison with previously published data, all potentials given in the text and in Table 5 have been converted to values relative to the saturated calomel electrode (SCE) according to the following relationship: $E(SCE) = E(Ag/AgNO_3) + 298$ mV.

2.2. Synthesis

2.2.1. Synthesis of 4-pyrrolidinopyridine

4-pyrrolidinopyridine (pypo) was prepared by using a modified reported literature method **[23]**. 9.4 g (0.1 mol) of 4-aminopyridine was dissolved in 100 mL of dimethylformamide then 27.6 g (0.2 mol) of potassium carbonate was added. This mixture was cooled with ice and 14.1 g (0.1 mol) of 4-chlorobutyrate chloride was added and left for 30 more min. The mixture was then heated to 120 °C and stirred for 1 hour. 200 mL of ice water were poured into the reaction mixture and then extracted with chloroform. The chloroform phase was concentrated under reduced pressure to obtain crude crystals. The obtained solid was recrystallized with hexane and ethyl acetate to yield the 4-pyrrolidinopyridine (pypo) final product. Amount 10.5 g, Yield: 64%.H-NMR ($CDCl_3$), 5: 8.52 (d, 2H), 7.59 (d, 2H), 3.85 (t, 2H), 2.64 (t, 2H), 2.19 (m, 2H).

2.2.2. Synthesis of [Mg(TTP)]

The *meso*-tetratolylporphyrin (H_2TTP) was prepared by using the Alder and Longo method **[24]**. The (*meso*-tetratolylporphyinato)magnesium(II) with the formula [Mg(TTP)] was prepared following a modified reported literature method **[25]**. 0.5 g (0.74 mmol) of H_2TTP was dissolved in 40 mL of dichloromethane. Then 1.35 g (5.25 mmol) $MgBr_2{\cdot}O(Et)_2$ were added and 2 mL (14 mmol) of triethylamine were added. The mixture was stirred under argon at room temperature for 1 hour. The [Mg(TTP)] complex precipitated after the addition of 40 mL of dichloromethane then the mixture was washed with distilled water. After decantation, 100 g of Na_2SO_4 was added to the organic phase then stirred for 1 hour. The solvent was removed and a solid of [Mg(TTP)] was obtained by precipitation in a
dichloromethane–n-hexane mixture (470 mg, 94%).

2.2.3. Synthesis of [Mg(TTP)(4-pypo)$_2$]·2CH_2Cl_2 **(I)**

[Mg(TTP)] (30 mg, 0.043 mmol) and 4-pyrrolidinopyridine (4-pypo) (90 mg, 0.608 mmol) were dissolved in 15 mL of dichloromethane and stirred at room temperature overnight. The color of the solution changed to green blue. The obtained compound crystallizes by slow diffusion of n-hexane through the dichloromethane solution to give after one week dark-blue crystals (43 mg, 86 %).

Elemental analysis calcd (%) for $C_{68}H_{60}Cl_4MgN_8O_2$, C 68.78, H 5.09, N 9.44; found: C 69.02, H 5.21, N 9.53; HRMS (ESI) (dichloromethane): *m/z* $[Mg(TTP)]^+$ calcd for $C_{48}H_{36}MgN_4$: 692.2796; found: 692.2789 ; *m/z* $[Mg(TTP)(L')]^+$ (L' = 4-pyrrolidin-1-yl-pyridine, $C_9H_{12}N_2$) calcd for

$C_{57}H_{48}MgN_6$: 840.3802; found 840.3793; *m/z* $[Mg(TTP)(4\text{-pypo})]^+$ calcd for $C_{57}H_{46}MgN_6O$: 854.3594; found 854.3583; UV–vis: λ_{max} (nm) in CH_2Cl_2: 427, 565, 606 ; FT-IR (solid neat): $\bar{\nu}$ (cm^{-1}) = 2981–2835 [CH Porph], 1738/1717 1600 cm^{-1} [ν(C=O) and [ν(C=N) porph)],1738 and 1717 [ν(C=O) 4-pypo ligand]; ^1H NMR (300 MHz, $CDCl_3$ δ (ppm): 8.84 (Hβ-pyrrol), 7.82 ($H_{o,o}$ Porph), 7.33 ($H_{m,m'}$ Porph), 8.06 (H_L 4-
pypo), 7.50 ($H_{L'}$ 4-pypo), 2.52 (H_g 4-pypo), 3.58 (H_e 4-pypo) and 2.09 (H_f 4-pypo).

2.3. X-ray structure determination

X-ray quality crystal of $[Mg(TTP)(4\text{-pypo})_2]\cdot 2CH_2Cl_2$ (**I**) were obtained by slow diffusion of n-hexane into a dichloromethane solution of complex **I**. Crystal evaluation and data collection were performed on a D8 VENTURE Bruker AXS diffractometer equipped with a CCD area detector with Mo Ka radiation (λ = 0.71073 Å). The crystals were kept at 150 (2) K during data collection. The data were scaled and corrected for absorption correction using SADABS-2004/1 (Bruker, 2004) **[26]**. The structure was solved by direct methods by using SIR-2004 **[27]** and refined by full-matrix least-squares techniques on F^2 by using the SHELXL-2014 program **[28]**. During the refinements of the structure of **I**, several disordered problems were encountered: (i) one phenyl group of "molecule 2" ([Mg2(TTP)$(4\text{-pypo})_2$]) is disordered in two positions (C77-C78A-C79A-C80-C81A-C82A and C77-C78B-C79B-C80-C81B-C82B) with refine occupancy factor of the major position of 0.593 (0.007), (ii) a first disordered dichloromethane solvent molecule presents three positions with occupancies being: 0.710 (0.003): 0.18731 (0.003): 0.102 (0.002) for C101-Cl3-Cl4, C102-Cl5-Cl6 and C103-Cl7-Cl8, respectively and (iii) a second dichloromethane is disordered in three positions (C104-Cl9-Cl10, C105-Cl11-Cl12 and C106-Cl13-Cl14) with refine occupancy factors of 0.561 (0.003): 0.336 (0.002): 0.103 (0.002), respectively. For the three disordered moieties, the anisotropic displacement ellipsoids of the disordered atoms are very elongated, which indicate that they are statistically disordered. Consequently, the SIMU and PLAT (for the disordered phenyl) restraints commands in the SHELXL-2014 software were used **[29]**. The DFIX and DANG constraint commands were also used to correct the geometry of these moieties **[30]**. For **I** non-hydrogen atoms were refined with anisotropic thermal parameters whereas H-atoms were included at estimated positions using a riding model. Drawings were made using ORTEP3 for windows **[31]** and MERCURY **[32]**. The crystallographic data and structural refinement details of **I** are shown in Table 1. Selected bond lengths and angles for this compound are listed in Table 2.

Table 1. Crystal data and structural refinement for $[Mg^{II}(TTP)(4\text{-pypo})_2]\cdot 2CH_2Cl_2$ (**I**).

Formula	$C_{68}H_{60}Cl_4MgN_8O_2$
M.W.	1187.40
Crystal System	triclinic
Crystal	*P-1*
a (Å)	13.099 (14)
b (Å)	19.5265 (19)
c (Å)	20.539 (2)
α (°)	62.193 (3)
β (°)	77.475 (4)
γ (°)	76.899 (4)
V (Å^3)	4487.9 (8)
Z	3
ρ_{calc}./ g.cm^{-3}	1.318
μ/ mm^{-1}	0.262
F(000)	1860
Crystal size (mm^3)	0.60 x 0.48 x 0.35
Crystal Color	purple
Crystal Shape	prism
T(K)	150 (2)
θ_{min} - θ_{max} (°)	2.940 – 26.000
Limiting indices	-16 ≤ h ≤ 16, -23 ≤ k ≤ 24, -25 ≤ l ≤ 25
R(int)	0.0434
Total/Unique data	92850/17621
Observed data [$I_o > 2\sigma(F_o)$]	13088
Parameters/Rest	1265/351
S [Goodness of fit]	1.066
R_1[a], wR_2[b] [$F_o > 4\sigma(F_o)$]	R_1 = 0.0837, wR_2 = 0.2110
wR_2[b] [all data]	R_1 = 0.1113, wR_2 = 0.2328
Min./max. res. (eÅ^{-3})	1.149 /-0.716
CCDC	2123511

[a] :$R1 = \Sigma||F_O|-|F_C||/\Sigma|F_O|$, [b] :$wR2 = \{\Sigma[w(|F_O|^2-|F_C|^2)^2]/\Sigma[w(|F_O|^2)^2]\}^{1/2}$.

Table 2. Selected bond lengths (Å) and angles (°) of **I**.

Magnesium Mg1 coordination polyhedron (molecule 1)

Mg1-N1	2.069(3)	N3-Mg1-N4	90.71(10)
Mg1-N2	2.068(3)	N5-Mg1-N1	91.39(10)
Mg1-N3	2.073(3)	N5-Mg1-N2	89.83(11)
Mg1-N4	2.069(3)	N5-Mg1-N3	88.20(10)
Mg1-N5	2.310(3)	N5-Mg1-N4	90.11(11)
Mg1-N7	2.292(3)	N7-Mg1-N1	89.01(10)
N1-Mg1-N2	90.83(10)	N7-Mg1-N2	89.47(11)
N1-Mg1-N3	179.53(11)	N7-Mg1-N3	91.40(11)
N1-Mg1-N4	89.05(10)	N7-Mg1-N4	90.59(11)
N2-Mg1-N3	89.40(11)	N7-Mg1-N5	179.20(11)
N2-Mg1-N4	179.86(11)		

Magnesium Mg2 coordination polyhedron (molecule 2)

Mg2-N9	2.076(3)	N9-Mg2-N10	90.93(12)
Mg2-N10	2.077(3)	N9-Mg2-N11	92.49(11)
Mg2-N11	2.302(3)	N10-Mg2-N11	90.42(11)

1-(pyridinyl)pyrrolidin-2-one (4-pypo) *Axial ligand (molecule 1)*

N5-C49	1.336(4)	N7-C58	1.342(4)
N5-C53	1.336(4)	N7-C62	1.331(5)
C49-N5-C53	115.7(3)	C58-N7-C62	115.4(3)
C49-N5-Mg1	124.2(2)	C58-N7-Mg1	120.1(2)
C53-N5-Mg1	119.5(2)	C62-N7-Mg1	124.2(2)
C51-N6	1.402(4)	C60-N8	1.396(5)
N6-C54	1.453(5)	N8-C63	1.449(6)
N6-C57	1.397(5)	N8-C66	1.405(6)
C54-N6-C57	112.3(3)	C63-N8-C66	112.2(4)
C50-C51-N6	121.2(3)	C63-N8-C60	121.9(4)
C52-C51-N6	121.2(3)	C66-N8-C60	125.4(4)
C57-O2	1.224(5)	C66-O1	1.235(6)
N6-C57-O2	126.3(4)	N8-C66-O1	125.8(4)
C56-C57-O2	126.6(4)	C65-C66-O1	126.6(4)

1-(pyridinyl)pyrrolidin-2-one (4-pypo) *Axial ligand (molecule 2)*

N11-C91	1.341(5)	N12-C99	1.350(7)
N11-C95	1.345(5)	C96-N12-C93	120.6(4)
C91-N11-C95	115.6(3)	C99-N12-C93	128.1(4)
C91-N11-Mg1	123.1(3)	C99-O3	1.168(8)
C95-N11-Mg2	120.9(2)	O3-C99-N12	124.9(5)
C93-N12	1.390(5)	O3-C99-C98	126.8(6)
N12-C96	1.481(6)		

2.4.Antifungal activity

2.4.1 Fungal strain and culture conditions

The antifungal effect of our three porphyrin derivatives was explored against yeasts from *Candida* genus from the American Type Culture Collection : *Candida albicans* (ATCC 90028), *Candida glabrata* (ATCC 64677) and *Candida tropicalis* (ATCC 66029) and two genus of dermatophytes : *Trichophyton rubrum* (MS 7793.1) and *Microsporum canis* (MS 8972), identified from clinical isolates by the professional team in the laboratory of parasitology and mycology of the teaching hospital Fattouma Bourguiba (Monastir-Tunisia). Before each antifungal assay, mycosic strains were maintained in culture on Sabouraud dextrose agar (Biolife) plates, at 30°C during 48 hours for *Candida* spp. and seven days for the dermatophytes.

2.4.2. Anticandidal activity

2.4.2.1. Determination of minimum inhibitory concentration (MIC) on *Candida* spp.

The determination of Minimum Inhibitory Concentration (MIC) of the porphyrins on the fungal strains was processed as described by Hrichi *et al.* **[33]**, using the microdilution method on flat bottom 96-well plates in the presence of Resazurin viability indicator. Briefly, the porphyrins were solubilized in dimethyl sulfoxide (DMSO) (m/v), and then adjusted in RPMI 1640 (PAN), supplemented by 2% glucose. Two hundred microliters of the porphyrin solution were added into the first well of each line of the 96-well plate, then 100 µL of RPMI 1640-2% glucose were dispensed in the remaining wells. A two fold serial dilution was applied from the first into tenth consecutive wells to obtain concentrations ranging from 10 to 78.10^{-2} $mg.mL^{-1}$. Thereafter, each well was inoculated with 90 µL of inoculum adjusted to $1\text{-}2.5.10^{5}$ UFC mL^{-1}. Then, 10 µL of resazurin indicator solution was added to a final volume of 200 µL per well. Positive (RPMI 1640-2% glucose with inoculum) and negative (RPMI 1640-2% glucose) control growth were included in all trials. Plates were then incubated at 37°C for 24 hours. Each experiment was run in triplicate. After incubation, the blue color indicates inhibition of growth, pink color indicates reduction of resorufin, and then persistence of strains. The lowest concentration which inhibited the visual growth was recorded as MIC.

2.4.2.2. Determination of minimum fungicide concentration (MFC) on *Candida* spp.

To determine the minimum fungicide concentration (MFC), 10 µL of each blue-stained well was loop spread onto Sabouraud Dextrose Agar (SDA) plates and incubated at the corresponding temperature. The concentration that induces no visible colonies or revealed three colonies or less to obtain approximately
99 to 99.5% killing growth after subsequent 7 days incubation was accepted as MFC.

2.4.3. Anti-dermatophytic activity

2.4.3.1. Anti-dermatophytic potential Screening

The *in vitro* anti-dermatophytic activity of porphyrins was screened by the agar incorporation technique in 24-well plates **[33]**. After a primer dissolution in DMSO (m/v), each porphyrin candidate was dissolved in 1 mL of SDA medium to obtain a final concentration of 10 mg. mL^{-1}. Well without substance was used as a negative control to monitor the growth of dermatophytes under normal conditions. Mycelial agar discs (2 mm) cut from an actively 7 days old growing culture of dermatophytes, were bored in the center of each petri dish. Each treatment consisted of triplicates. The percentage of growth inhibition of porphyrin was calculated by the formula :
% I inhibition = [growth in control - growth in sample/ growth in control] × 100.

2.4.3.2. Evaluation of the mycelial radial growth of dermatophytes

Three concentrations (5 $mg.mL^{-1}$, 2.5 $mg.mL^{-1}$ and 1.25 $mg.mL^{-1}$) of porphyrins with proven antifungal potential were incorporated in a final volume of 3 mL of SDA medium. A petri dish without substance was used as a negative control to monitor the growth of dermatophytes under normal conditions. Mycelial agar discs (2 mm) cut from the actively growing culture of 7 days old, were bored in the center of each petri dish. Each treatment consisted of triplicates. Petri dishes were sealed with Parafilm to avoid dehydration. In that method radical growth was three-time interval measured for each concentration.

The percentage of growth inhibition of porphyrin was calculated by the formula:

% I inhibition = [growth in control - growth in sample/ growth in control] × 100.

3. Results and Discussion

3.1. Synthesis of $[Mg(TTP)(pypo)_2]\cdot 2CH_2Cl_2$ (I)

Complex **I** was prepared by reacting the [Mg(TTP)] starting material with an excess of 1-(pyridinyl)pyrrolidin-2-one (4-pypo) in dichloromethane at room temperature (Scheme 1). Our Magnesium(II)-TTP-bis(pypo) derivative was isolated in a 87% yield using a slow diffusion of n-hexane in the dichloromethane solution. According to the elementary analysis the formula of **I** is $[Mg(TTP)(pypo)_2]\cdot 2CH_2Cl_2$.

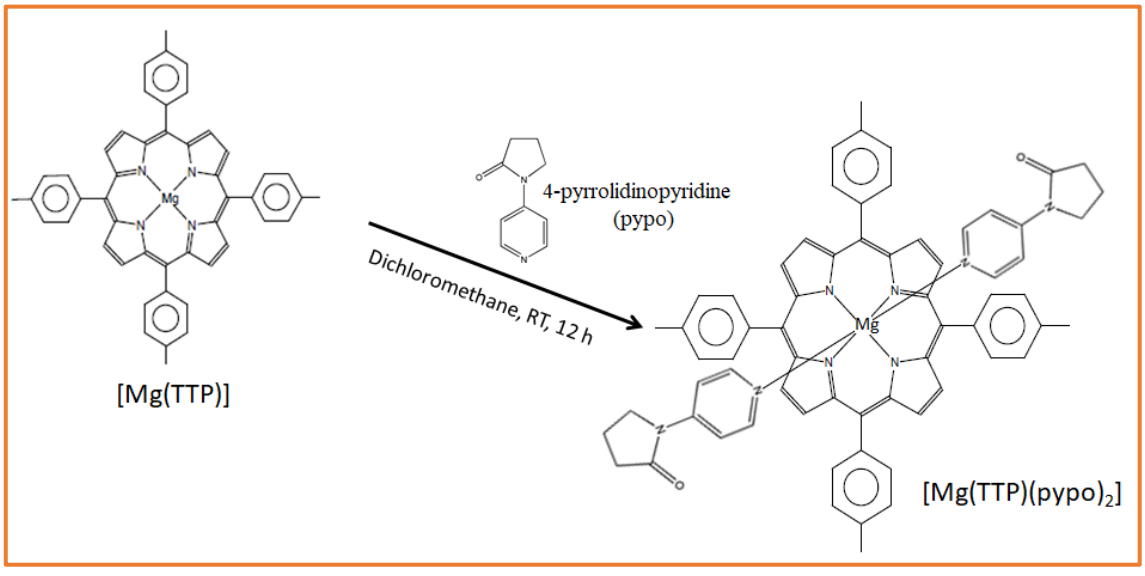

Scheme 1. Scheme of the synthesis of $[Mg(TTP)(4\text{-}pypo)_2]\cdot 2CH_2Cl_2$ (**I**).

3.2. ^{1}H NMR and IR spectroscopy

The ^{1}H NMR data of the H_2TTP free base porphyrin, the [Mg(TTP)] starting material are depicted in Figures S1 and S2 and that of corresponding to compound **I** is shown in Figure 1. The chemical shift of the β-pyrrole protons (H_β), the phenylic protons ($H_{o,o'}$, $H_{m,m'}$) values are 8.84, 7.82 and 7.33 ppm are characteristic for diamagnetic *meso*-arylmetalloporphyrins with zinc(II), magnesium(II) and cadmium(II) as center ions **[34-36]**. As illustrated by Figure 1, the 1-(pyridinyl)pyrrolidin-2-one (4-pypo) axial ligand presents pyridyl protons (H_L and H'_L) and pyrrolidine-2-one protons (H_g, H_e and H_f) signals at 8.06, 7.50, 2.52, 3.58 and 2.09 ppm, respectively. The reported non-coordinated 1-(pyridinyl)pyrrolidin-2-one (4-pypo) H_L , H'_L, Hg, He and Hf protons resonate at 8.52, 7.59, 2.62, 3.85 and 2.19 ppm which slightly different from those of the coordinated 4-pypo axial ligand. Therefore the ^{1}H NMR investigation confirms the coordination of the 4-pypo ligand to the magnesium(II) of **I** in solution.

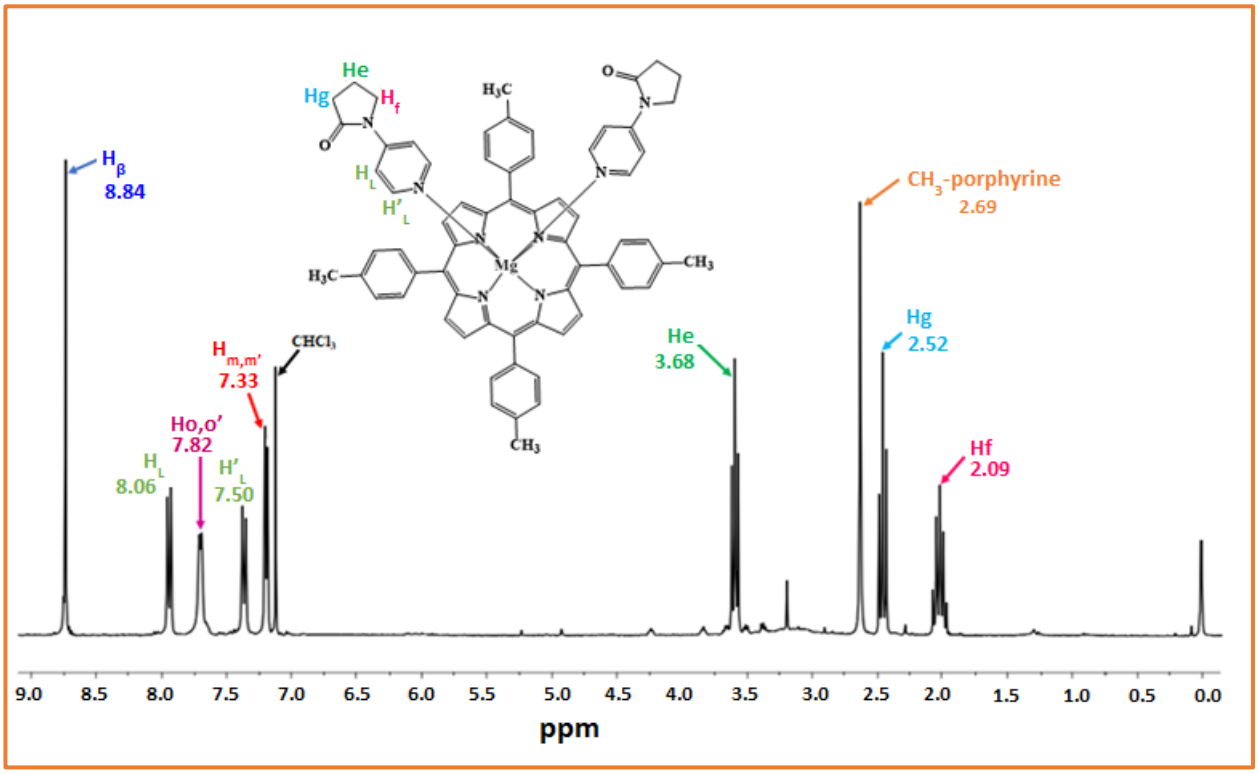

Figure 1. ^{1}H NMR spectrum of [Mg(TTP)(4-pypo)$_2$]·2CH_2Cl_2 (**I**) recorded in $CHCl_3$ at room temperature with concentration C ~10^{-3} M.

Figure S3 illustrates the IR spectrum of the H_2TTP free base porphyrin while Figure 2 presents both spectra of the [Mg(TTP)] starting material and **I**. In the IR spectrum of [Mg(TTP)] we noticed

the disappearance of the weak absorption band at 3310 cm^{-1}, attributed to the ν(NH) stretching of the pyrrole rings of the TTP porphyrinate, and the shift toward the high frequencies of the δ(CCH) band from 968 (free base porphyrin) to 995 cm^{-1} ([Mg(TTP)] indicating the metalation of the H_2TTP porphyrin. The coordination of the 1-(pyridinyl)pyrrolidin-2-one (4-pypo) to [Mg(TTP)] leading to complex **I** is confirmed by two strong absorption bands at 1738/1717 1600 cm^{-1} attributed to the ν(C=O) and ν(C=N) stretching frequencies (Figure 2). The presence of two absorption bands at 1738 and 1717 cm^{-1} attributed to the ν(C=O) of the 4-pypo axial ligand is a consequence of the coordination of this ligand to Mg1 and Mg2 center metals in molecules 1 and 2 respectively (see crystallographic section).

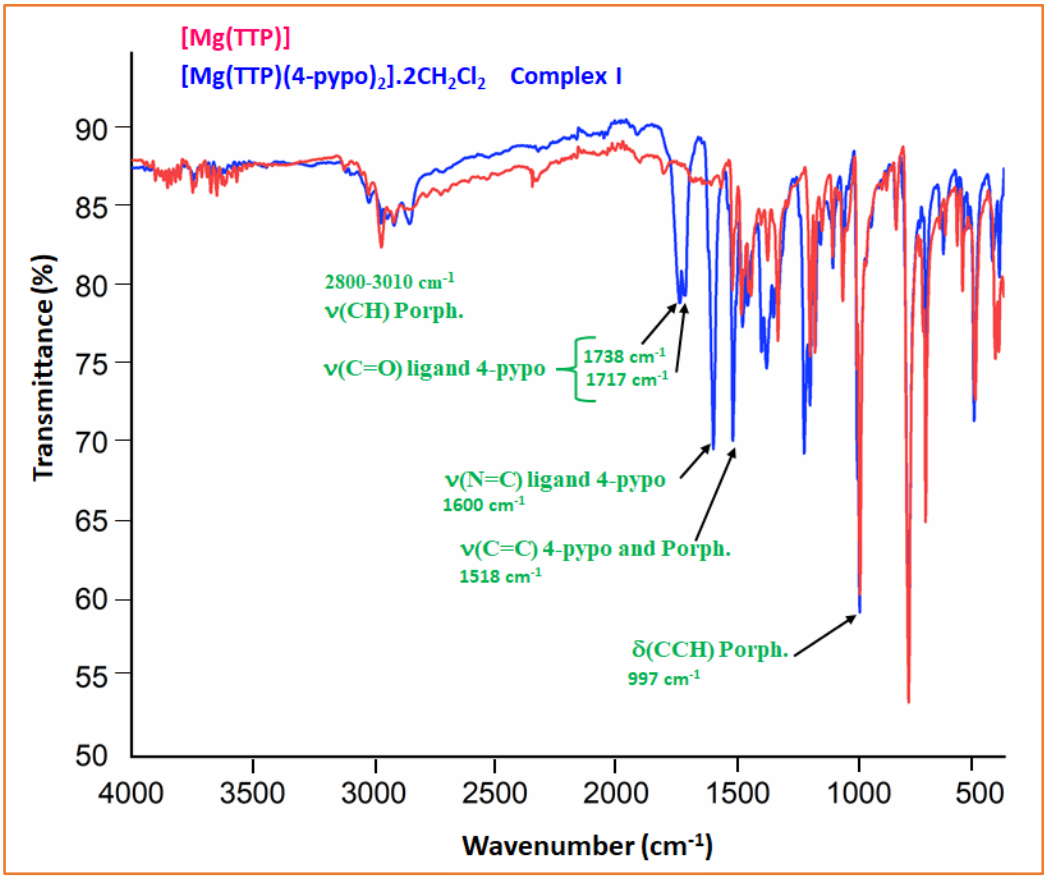

Fig. 2. Neat IR spectrum of [Mg(TTP)] staring material (red color) and [Mg(TTP)(4-pypo)$_2$]·2CH_2Cl_2 (**I**) (blue color).

3.3. ESI-HRMS mass study on [Mg(TTP)(4-pypo)$_2$]·2CH_2Cl_2 (I)

Figure 3 represents the ESI-HRMS mass spectrum solution of **I** in positive ion mode recorded in a dichloromethane which shows the presence of the three following fragments: (i) fragment (a)

corresponding to $[Mg(TTP)]^+$ with experiment ant theoretical m/z values of 692.2789 and 692.2796, respectively, (ii) fragment (b) attributed to $[Mg(TTP)(L')]^+$ for which L' is the 4-pypo ligand without the oxygen atom (L' = 4-pyrrolidin-1-yl-pyridine, $C_9H_{12}N_2$) with experimental and theoretical m/z values are 840.3793 and 840.3802, respectively, and (iii) fragment (c) corresponding to [Mg(TTP)(4-pypo)] with experimental and theoretical m/z values 854.3583 and 854.3595, respectively. Therefore, this technique shows that in solution, at least, one 4-pypo axial ligand is coordinated to Mn(II) in compound **I**. Experimental and simulated isotopic pattern of **I** in the m/z region attributed to the $[Mg(TPP)(4\text{-pypo})]^+$ is shown in Figure S4.

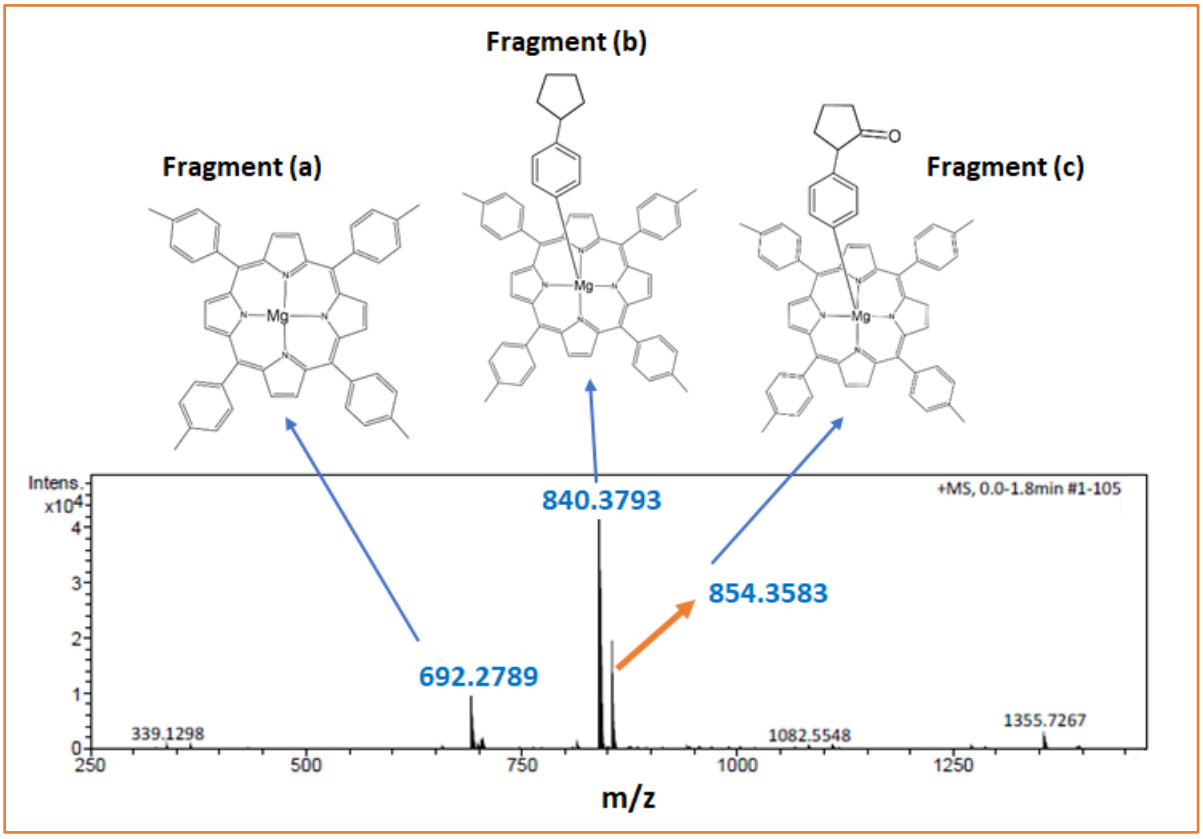

Fig. 3. ESI-HRMS spectrum of $[Mg(TTP)(4\text{-pypo})_2].CH_2Cl_2$ (**I**). Spectrum recorded in dichloromethane with a concentration of 5.10^{-3} M.

3.4. Photophysical properties

In Figure 4 are shown the electronic absorption spectra of H_2TTP, [Mg(TTP)] and **I**. The H_2TTP free base porphyrin presents a Soret band at 420 nm and four Q bands at 518, 554, 593 and 649 nm. The metalation of the porphyrin leads to a redshift of the Soret band with λ_{max} values of 428 and 427 nm for [Mg(TTP)] and complex **I**, respectively and the number of the Q bands is reduced from four to two due to the change of the symmetry from D_{4h} to D_{2h}. The λ_{max} values of these Q bands are 566, 607 nm and 565 and 606 nm for [Mg(TTP)] and **I**, respectively. These data show

that the coordination of 4-pypo to the Mg(II) center metal didn't lead to a noticeable change of the UV-Vis spectrum of the [Mg(TTP)] starting material. This has been also seen for related pentacoordinated and hexacoordinated and Mg(II) *meso*-aryporphyrins such as [Mg(TClPP)(DMAP)] (TClPP = *meso*-tetra(*para*-chlorophenyl)porphyrinate and DMAP = 4-(dimethylamino)pyridine **[12]** and [Mg(TPBP)(HTMA)$_2$] (TPBP = *meso*-tetrakis[4(benzoyloxy)phenyl]porphinate and HMTA = hexamethylenetetramine) **[10]**.

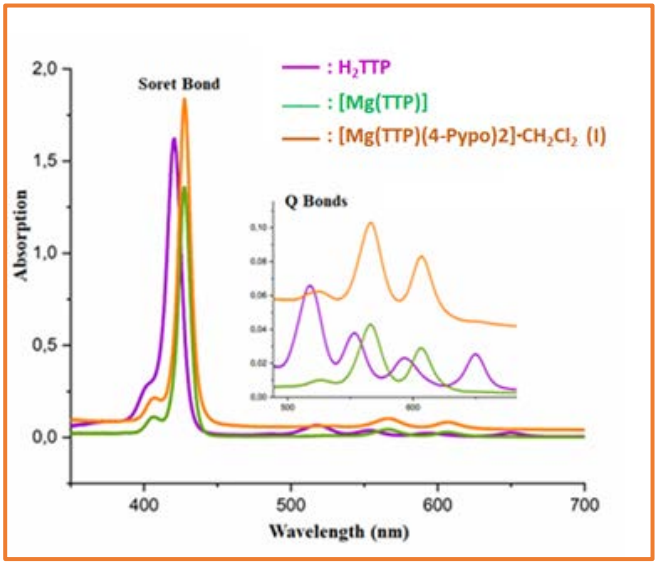

Fig. 4. UV-Vis spectra of H_2TTP, [Mg(TTP)] and [Mg(TTP)(4-pypo)$_2$]·CH_2Cl_2 (**I**) recorded in dichloromethane with concentration ~ 10^{-6} M.

The emission spectra of porphyrins and metalloporphyrins exhibit two emission transitions: $S_1 \rightarrow S_0$ and $S_2 \rightarrow S_0$ allocated as the Q(0,0) and Q(0,1) transitions where S_0, S_1 and S_2 are the ground state, the first and the second excited states, respectively. The $S_2 \rightarrow S_0$ transition concerns the Soret band is usually neglected because for of its very weak intensity compared to that of the $S_1 \rightarrow S_0$ transition. In Figure 5, is depicted the emission spectra of our three porphyrinic species: H_2TTP, [Mg(TTP)] and [Mg(TTP)(4-pypo)$_2$]·$2CH_2Cl_2$ (**I**). These spectra were recorded at room temperature in dichloromethane with concentrations ~10^{-6} M under an excitation wavelength of 450 nm. The λ_{max} values of the the Q(0,0) and Q(0,1) fluorescence bands, the fluorescence quantum yields (ϕ_f) and the fluorescence lifetimes (τ_f) of our three porphyrin compounds and a selection of *meso*-arylporphyrins and metalloporphyrins are summarized in Table 3. The λ_{max} values of the O(0,0) and Q(0,1) emission bands of the H_2TTP free base are 657 and 721 nm which are in the range 652 – 720 nm of free base *meso*-arylporphyrins (Table 3). The metalation of the H_2TTP porphyrin par Mg(II) leads to an important blue-shift of the Q(0,0) (46 nm) and the Q(0,1)

(66 nm) bands compared to those of the free base porphyrin. The coordination of the 4-pypo ligand to the magnesium(II) center metal of [Mg(TTP)] has a minor effect on the positions of the Q bands (Figure 5, Table 3).

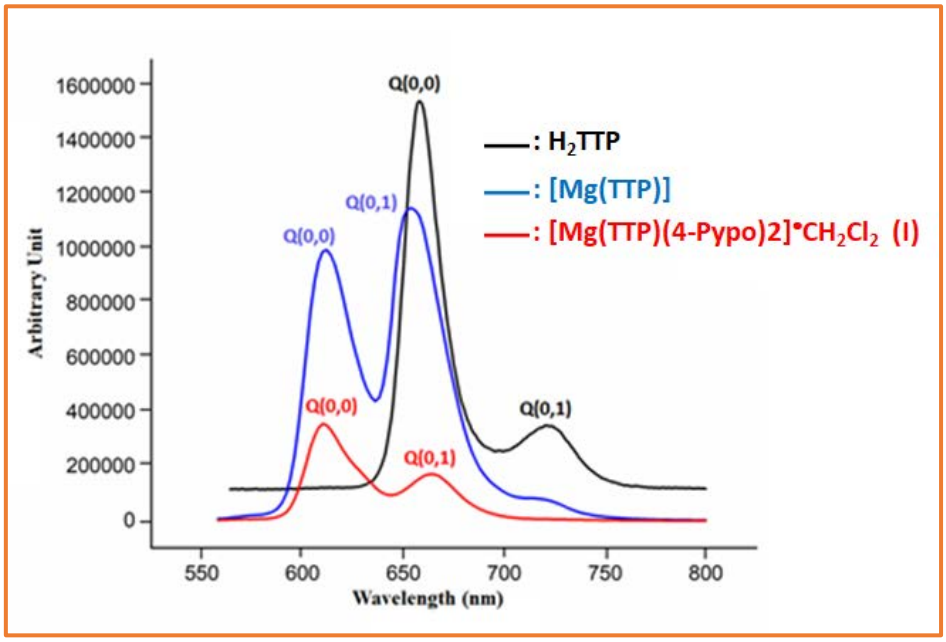

Fig. 5. Fluorescence spectra of H_2TTP, [Mg(TTP)] and [Mg(TTP)(4-pypo)$_2$]·CH_2Cl_2 (**I**) recorded in dichloromethane with concentration ~ 10^{-6} M. λ_{max} of the excitation wavelength is 450 nm.

Noteworthy, the λ_{max} values of Q(0,0) and Q(0,1) of the three divalent center metals Mg(II), Zn(II) and Cd(II) metalloporphyrins, which are diamagnetic, are close and in the domain 694 – 625 nm for the Q(0,0) band and 643 – 670 nm for the Q(0,1) band (Table 3). The fluorescence quantum yields (Φ_f) and the fluorescence lifetimes (τ_f) values of the free base H_2TTP porphyrin are ~10% and 7.90 ns, respectively which are in the normal range of *meso*-porphyrins. These values increase after metalation of H_2TTP by Mg(II) ([Mg(TTP)]) and addition of the 4-pypo axial ligand (**I**) with Φ_f and τ_f values of 15%/13% and 9.10/4.6 nm, respectively. It is noteworthy that (i) for zinc(II) *meso*-arylporphyrins the Φ_f are in the range 1% - 4.6% and the τ_f values range between 1.5 and 4.2, (ii) cadmium(II) *meso*-arylporphyrins exhibit fluorescence quantum yields fluorescence lifetimes values much smaller than those of both zinc(II) and Mg(II) porphyrin species. This is mainly due to the high molar mass of Zn(II) and especially Cd(II) center ions leading to a quenching effect, resulting in the very low Φ_f values **[37]**.

Table 3. Emission data for H_2TTP, [Mg(TTP)], [Mg (TTP)(4-pypo)$_2$]·2CH_2Cl_2 (**I**) and a selection of *meso*-tetraarylporphyrins comlpounds.

Compound	λ_{max} (nm)		Φ_f	τ_f (ns)	Ref.
	Q(0,0)	Q(0,1)			
Meso-arylporphyrins					
H_2TPP[a]	653	722	0.12	9.60	**[38]**
H_2TClPP[b]	652	714	0.089	7.72	**[12]**
H_2TMPP[c]	656	719	0.082	7.20	**[39]**
H_2TTP	657	721	0.098	7.90	t.w.
Mangnesium(II) meso-arylporphyrins					
[Mg(TPP)][a]	608	661	0.15	9.2	**[38]**
[Mg(TClPP)][b]	615	670	0.18	6.3	**[12]**
[Mg(TTP)]	611	655	0.15	9.1	t.w.
[Mg(TTP)(NCO]$^-$	609	664	0.18	3.8	**[8]**
[Mg(TPP)(THF)$_2$][a,d]	609	660	0.16	8.9	**[40]**
[Mg(TClPP)(DMAP)][b,e]	608	659	0.16	5.0	**[12]**
[Mg(TPP)(4,4'-dipy)$_2$][b,f]	613	668	0.13	4.9	**[41]**
[Mg(TPP)(HMTA)$_2$][a,g]	620	665	0.14	4.7	**[42]**
[Mg(TTP)(4-pypo)$_2$] (**I**)	611	663	0.13	4.6	t.w.
Zinc(II) meso-arylporphyrins					
[Zn(TPP)(N_3)]$^-$ [a]	594	643	0.036	1.7	**[12]**
[Zn(TTP)(mbpy)~py)][i]	611	652	0.021	–	**[43]**
[Zn(TPP)(IQNO)][a,j]	602	656	–	1.9	**[44]**
[Zn(TPP)(1,4-dioxane)$_2$][a]	604	655	–	1.8	**[45]**
Cadmium(II) meso-arylporphyrins					
[Cd(TBPP)(2-MeIm)][k,l]	612	657	0.02	1.7	**[36]**
[Cd(TMPP)(DABCO)][c,m]	625	652	0.01	1.2	**[46]**
[Cd(TClPP)(2-NH_2Py)][b,n]	618	653	0.04	4.2	**[47]**

[Cd(TClPP)(morph)][b,o]	619	654	0.046	1.5	**[48]**

[a]: H_2TPP = *meso*-tetraphenylporpyrin, [b]: H_2TClPP = *meso*-tetra(4-chlorophenyl)porphyrin, [c]: H_2TMPP = *meso*-tetra(4-methoxyphenyl)porphyrinate, [d]: THF = tetrahydrofuran, [e]: DMAP = 4-dimethylaminopyridine, [f]:4,4'-dipy = 4,4-bipyridine, [g]: HMTA = hexamethylenetetramine, [i]: mbpy)~py = 4-methyl-4-[2-(4-pyridyl)ethenyl]-2,2-bipyridine, [j]: IQNO = isoquinoline N-oxide, [k]: 1,4-dioxane = TBPP = meso-tetrakis(4-tert-butylphenyl)porphyrinate, [l]: 2-MeIm = 2-methylimidazole, [m]: DABCO = 1,4-diazabicyclo[2.2.2]octane, [n]: 2-NH_2Py = 4,4'-diaminodiphenylmethane. [o]: morph = morpholine.

3.5. X-ray Structure of I

In Table 1 are summarized the crystal data and structure refinement parameters of **I** while in Table 2 is reported a selection of the coordination polyhedral of magnesium center metal. This Mg(II) porphyrinic complex crystallizes in the triclinic group system with P-1 space group. The asymmetric unit of **I** is made by one and half [Mg(TTP)(pypo)$_2$] molecules and three disordered dichloromethane solvent molecule (Figure S5) indicating that the formula of complex **I** is [Mg(TTP)(pypo)$_2$]·2CH_2Cl_2. Figure 6 is an ORTEP drawing of molecule 1 ([Mg1(TTP)(4-pypo)$_2$]) and molecule 2 ([Mg2(TTP)(4-pypo)$_2$]).

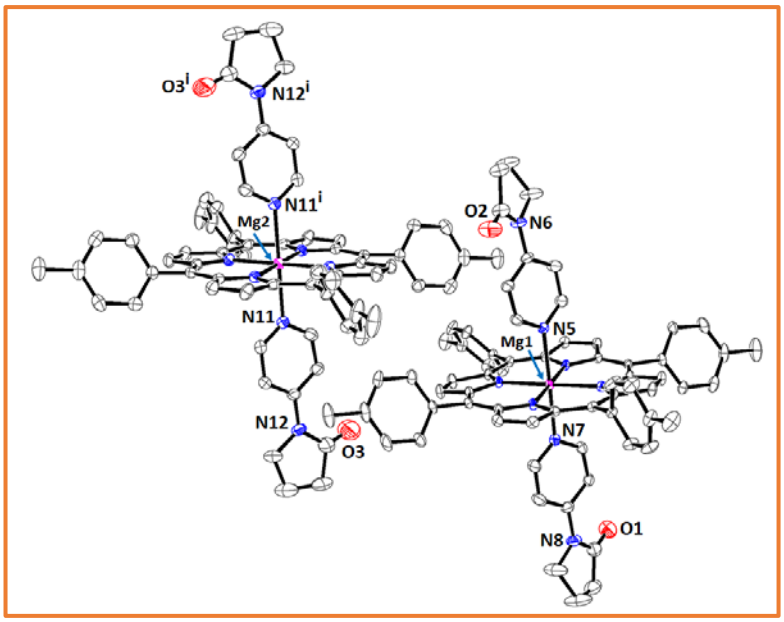

Fig. 6. Ortep drawing of molecules 1 and 2 of **I** with thermal ellipsoids drawn at 40% probability. The hydrogen atoms are omitted for clarity. Atoms label with **i** indices are the inversion center symmetry related atoms.

The average equatorial distance between the magnesium(II) center atom and the nitrogen atoms of the porphyrin ring (Mg—Np) is 2.070 (3) Å for molecule 1 and 2.076 (3) Å for molecule 2. These values are very close to the related pentacoordinate magnesium(II) *meso*-arylporphyrins type [Mg(Porph)(L)] (Porph = *meso*-arylporphyrinate and L is a neutral unidentate axial ligand) with

a Mg—Np distance ~ 2.070 Å. For hexacoordinated magnesium porphyrin complexes type [Mg(Porph)$(L)_2$], the Mg—Np distances are higher than those of the related pentacoordinated species (Mg—Np ~ 2.090 Å) which is explain by the fact that the porphyrin macrocycles of the pentcoordinated [Mg(Porph)(L)] coordination compounds exhibit usually a dome deformation leading to a lengthening of the Mg—Np distance (Table 4) **[49]**.

The Mg(II)—N(4-pypo) bond lengths are 2.310 (3) and 2.292 (3) for molecule 1 and 2.302 (3) Å for molecule 2. These values are close to the magnesium-substituted pyridines metalloporphyrins distances (Mg—N(py) and Mg—N(4-Mepy) of complexes [Mg(TPP)$(py)_2$] and [Mg(TPP)(4-Mepy)$_2$], respectively **[49,50]**.

The coordination polyhedral of the magnesium center atom of molecules 1 and 2 of **I** (Figure 7) show inter alia, that both two porphyrin cores are practically planar and that the pyridyl groups of the two 4-pipo axial ligands are parallel.

Table 4. Selected bond lengths [Å] and angles [°] for [Mg(TTP)$(4\text{-pypo})_2$]·$2CH_2Cl_2$ (**I**) and a selection of related Mg(II) *meso*-arylporphyrins.

Complex	Mg—X_L[a]	Mg__N_p[b]	Ref.
Pentacoordinated magnesium(II) meso-arylporphyrins			
[Mg(TClPP)(DMAP)][c,d]	2.130 (4)	2.082 (3)	**[12]**
[Mg(TBrPP)(HIm)][e,f]	2.120 (3)	2.094 (2)	**[9]**
[Mg(TPP)(H_2O)][g]	2.012 (6)	2.092 (7)	**[51]**
[K(222)][Mg(TPP)(N_3)][g,h]	1.997 (2)	2.1187 (16)	**[8]**
Hexacoordinated magnesium(II) meso-arylporphyrins			
[Mg(TPP)$(pipz)_2$][g,i]	2.423	2.073	**[49]**
[Mg(TPP)$(py)_2$][g,j]	2.376	2.072	**[50]**
[Mg(TPP)$(1\text{-MeIm})_2$][g,k]	2.297	2.079	**[49]**
[Mg(TPP)$(H_2O)_2$][g]	2.213	2.071	**[52]**
[Mg(TPP)$(4\text{-Mepy})_2$][l]	2.385	2.070	**[49]**
[Mg(TTP)$(4\text{-pypo})_2$] (**I**)	2.310 (3) / 2.292 (3)*	2.070 (3)*	this work
	2.302 (3)**	2.076 (3)**	

[a]: M—N_p = average equatorial cobalt-nitrogen pyrrole distance, [b]: M—X_L = metal-axial ligand distance, [c]: TClPP = *meso*- tetra(*para*-chlorophenyl)porphyrinate, [d]: DMAP = 4-(dimethylamino)pyridine, [e]: TBrPP = *meso*-tetrakis(4-bromophenyl) porphyrinato, [f]: Him = imidazole, [h]: [K(222] = (cryptand-222)potassium(+), [i]: pipz = piperazine, [j]: py = pyridine, [k]: 1-MeIm = 1-methylimidazole, [l]: 4-Mepy = 4-methylpyridine or 4-picoline-N.
*: for the full molecule 1, **: for the half molecule 2.

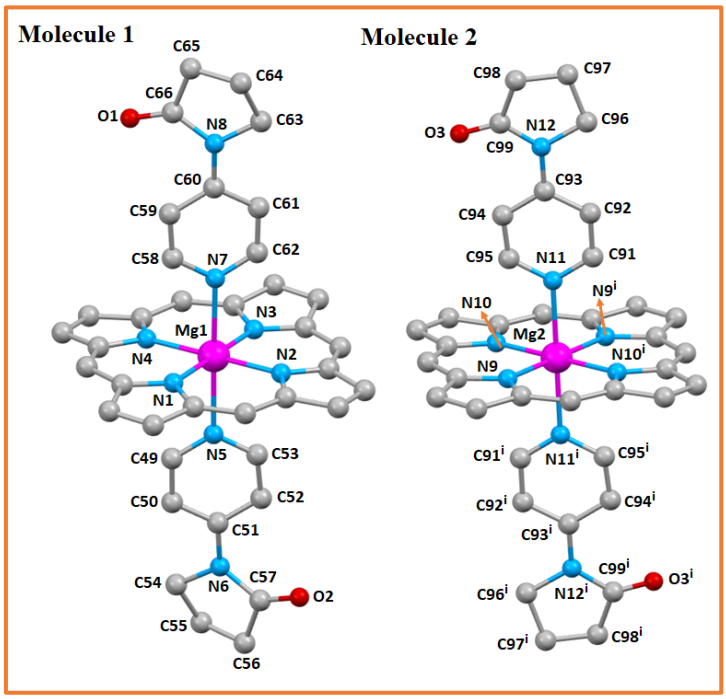

Fig. 7. Drawings showing the "porphyrin core – trans pypo ligands" moiety of molecules 1 and 2.

Figure 8 illustrates a part of the packing diagram of **I** down the *a* axis. The two complexes [Mg1(TTP)(4-pypo)**2**] (molecule 1) and [Mg2(TPP)(4-pypo)$_2$] (molecule 2) and the dichloromethane solvent molecules of **I** are linked together via weak intermolecular interactions as follows (Table S1, Figure 9, S6 and S7): (i) the three parts discorded solvent molecule (C101-Cl4-Cl5, C102-Cl5-Cl6, C103-Cl7-Cl8)) is H-bonded to the neighboring [Mg(TTP)(4-pypo)$_2$] molecules with C102-H10C-O2, C101-H10C-O2 and C103-H10-Cg3 (Cg3 is the centroid of C77-C78A-C79A-C80-C81A-C82A phenyl ring) and the oxygen O1 of the 4-pypo axial of a nearby [Mg(TTP)(4-pypo)$_2$] molecule are weakly H-bonded together with a C100-H100-O1 distance of 3.231 (6) Å, (iii) the other three parts disordered dichloromethane molecule (C104-Cl9-Cl10, C105-Cl11-Cl12, C106-Cl13-Cl14) is linked to the oxygen atom O3 of a 4-pypo axial ligand of a close by [Mg(TTP)(4-pypo)$_2$] and Cg12 centroid of the C35-C36-C37-C38-C39-C40 phenyl ring for a nearby TTP porphyrin (Table S1) and (iv) the carbon atoms C56 and C65 of two [Mg(TTP)(4-pypo)$_2$] molecules are weakly H-bonded to the Cg17 and C19 centroids of the N5/C49-C53 pyrrole ring and the N11/C91-C95 pyridyl ring of the 4-pypo axial ligand, respectively (Table S1).

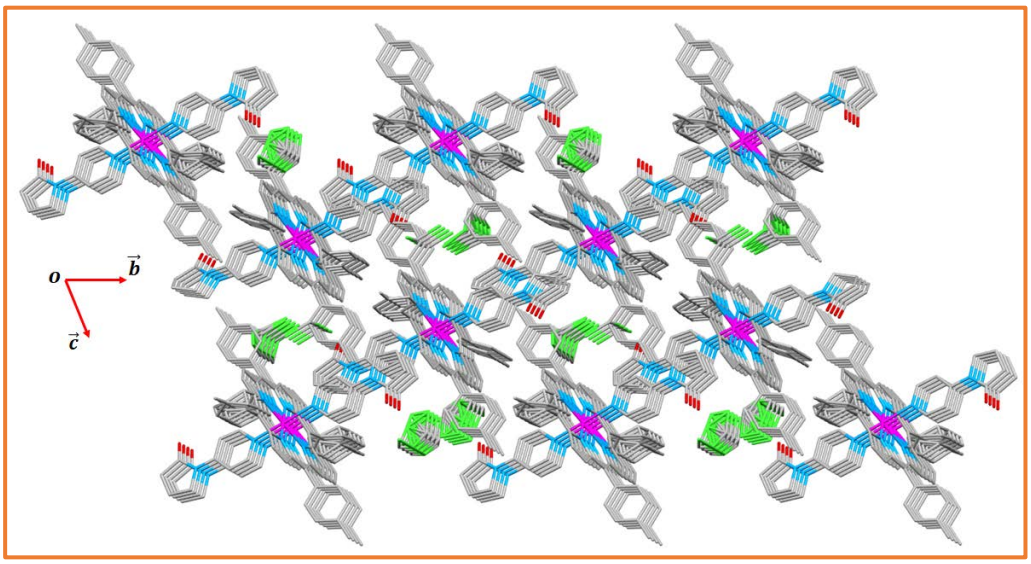

Fig. 8. Projection down the *a* axis of the crystal packing of **I**.

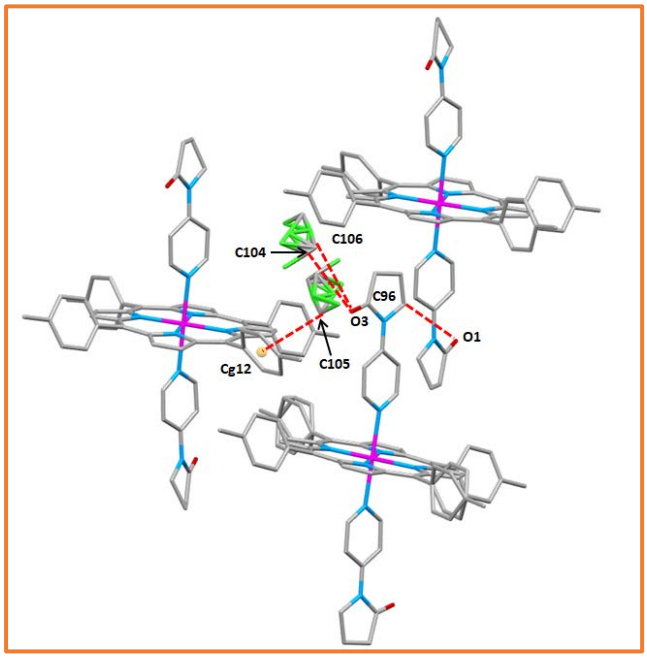

Fig. 9. The crystal structure of **I** showing the C–H···C, C–H···Cl and C–H···Cg intermolecular interactions.

3.6. Hirshfeld Surface Analysis

To further investigate the intermolecular interactions present in **I**, we performed a Hirshfeld surface analysis and the two-dimensional fingerprint plots were generated with Crystal Explorer17 **[53]**.

The red spots on the Hirshfeld surface indicate the presence of close contacts, whereas areas without close contacts are shown as blue spots. In Figure 10 is depicted the Hirshfeld surface of **I** mapped over the d_{norm} range from –0.7349 to 1.4964 Å. The 2D fingerprints plots (d_i versus d_e) along with the corresponding Hirshfeld surface of **I** (Figure 11) present intermolecular contacts between atom interactions and show percentage of contributions from different interaction types. The H…H, H…C/C…H, H…Cl/Cl…H have the most important contribution to the total Hirshfeld surface with 59.2% and 17.1%, respectively. For the O…H/O…H and Cl…C/C…Cl interactions present 4.9% and 2.3% of the total map, respectively.

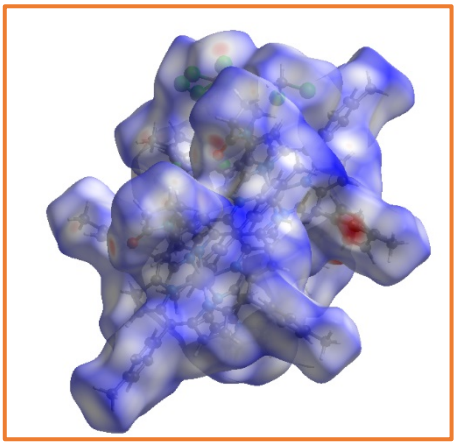

Fig. 10. Hirshfeld surfaces of complex **I** mapped over d_{norm}.

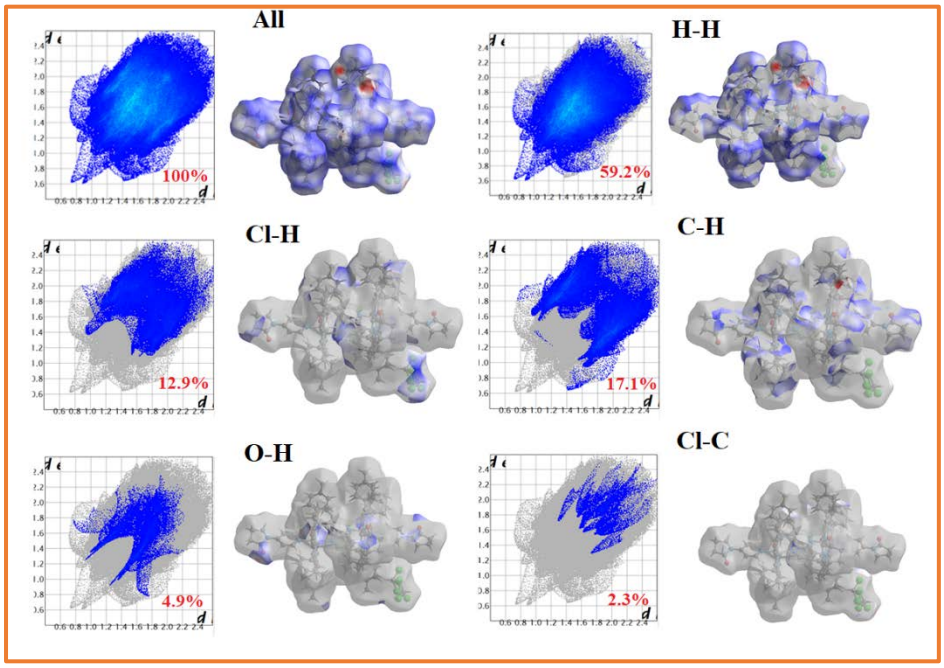

Fig. 11. Hirshfeld surface mapped over d_{norm} and decomposed fingerprint plots for the dominant interactions in **I**.

3.7. Cyclic voltammetry

Il is known that cyclic voltammograms of porphyrin complexes with non-electroactive divalent metal center ions such as Mg(II), Zn(II) and Cd(II) present usually two or three reversible one-electron oxidation waves and one or two one-electron reversible (or irreversible) reduction waves attributed to the porphyrin macrocycle **[8,35,12]**. The cyclic voltammogram of **I** (Figure 12, Scheme 2, Table 5) presents one one-electron reversible reduction wave with half potential value ($E_{1/2}$) (R4/O4) of -1.60 V and three reversible one-electron oxidations waves with $E_{1/2}$ values of 0.62 (O1,R1), 1.04 (O2,R2) and 1.26 V (O3,R3). We notice that the $E_{1/2}$ values of the three oxidation waves of **I** are very close to those of the related Mg(II) porphyrins reported in Table 5 while the $E_{1/2}$ value of the reduction wave of our Mg-TTP-bis(4-pypo) derivative is slightly shifted toward the negative potentials compared to the other related Mg(II) species. This indicates that **I** is harder to reduce. This cyclic voltammetry investigation shows that the electrochemical data of Mg(II) porphyrins did not depends to either the nature of the group present in the *para* position of the *meso*-arylporphin (H for TPP, CH_3 for TPP and Cl for TClPP) nor the type of the N-donor axial ligand [N^{3-}: azido, HMAT: hexamethylenetetramine of 4-pypo: 1-(pyridinyl)pyrrolidin-2-one).

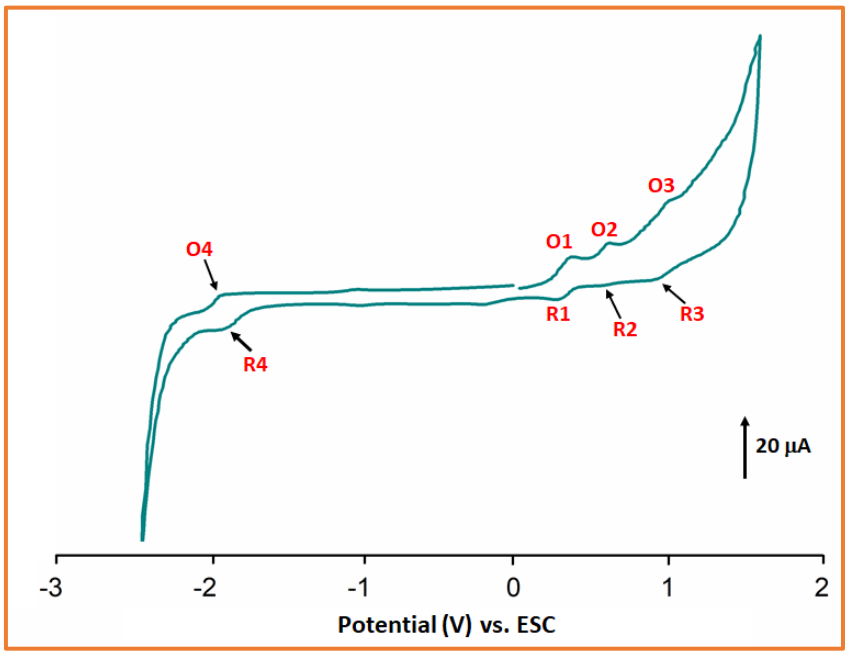

Fig.12. Cyclic voltammogram of $[Mg(TTP)(4\text{-pypo})_2]\cdot 2CH_2Cl_2$ (**I**). The solvent used is dichloromethane, and the concentration is ca. 10^{-3} M in 0.2 M TBAP, 50 mV/s, vitreous carbon working electrode (Ø = 3 mm).

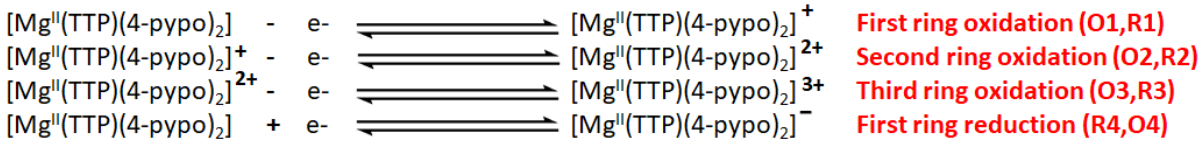

Scheme 2

Table 5. Potentials (in V vs SCE) of investigated **I** and a selection of related manganese(II) *meso*-arylmetalloporphyrins.

Compound	Oxidation			Reduction	Ref.
	Metal Oxid. (O1,R1)	1st Porph. Oxid. (O2,R2)	2nd Porph. Oxid. (O3,R3)	1st Porph. Red. (R4,O4)	
	$E_{1/2}$[a]	$E_{1/2}$[a]	$E_{1/2}$[a]	$E_{1/2}$[a]	
$[Mg(TPP)(N_3)]^{-}$[,b]	0.57	0.89	1.15	–1.52	**[8]**
$\{[Mg(TPP)(pyz)]\}_n$[b,c]	0.65	0.95	-	–1.65	**[11]**
$[Mg(TPP)(HMTA)_2]$[a,d]	0.73	0.99	-	–1.45	**[42]**
[Mg(TClPP)(DMAP)][e,f]	0.63	0.91	1.22	–1.42	**[12]**
$[Mg(TTP)(4\text{-pypo})_2]$ (**I**)	0.62	1.04	1.26	-1.60	t.w.

[a]: $E_{1/2}$ = half-wave potential, [b]: TPP = *meso*-tetraphenylporpyrinte, [c]: pyz = pyrazine, [d]: HTMA = hexamethylenetetramine, [e]: TClPP = *meso*-tetra(**4**-chlorophenyl)porphyrinate, [f]: DMAP = 4-dimethylaminopyridine.

3.8. Antifungal activity

3.8.1. Antidermatophyte activity

The free base porphyrin H_2TTP and complexes [Mg(TTP)] and [Mg(TTP)(4-pypo)$_2$]·2Cl$_2$Cl$_2$ (**I**) were evaluated for their *in vitro* antifungal activity against five pathogenic fungi : three yeasts strains (*C. albicans ATCC90028, C. glabrata (ATCC 64677)* and *C. tropicalis (ATCC 66029)* and two dermatophytes' strains (*trichophyton rubrum (MS 7793.1* and *Microsporum canis (MS 8972)*). We first tested our porphyrin derivatives against *Candida spp*. Anticandidal activities of the porphyrin species were determined by microdilution method by determining MIC and MFC values. MIC and MFC values were presented in the Table 6.

[Mg(TTP)(4-pypo)2]·2CH$_2$Cl$_2$ (**I**) shows the best activity against all the three strains of *Candida* spp. *C. albicans, C. glabrata* and *C. tropicalis* with MIC values in the range of 2.5 mg.mL^{-1} to 10 µg.mL^{-1}. This species presents a fungicidal potential with MIF values ranging from 5 to >10 mg.mL^{-1}.

A lower antifungal potential was observed for H_2TTP free porphyrin and [Mg(TTP)], which present fungistatic concentrations (MIC) values starting from 5 mg mL^{-1} and fungicidal yields (MFC) almost higher than 10 mg.L^{-1} against the three *Candida* species.

Table 6. Minimum inhibitory concentration (MIC) and minimum fungicidal concentration (MFC) of the three 3 porphyrin derivatives against yeasts strains.

Porphyrin compound	*Candida albicans* (ATCC 90028)		*Candida glabrata* (ATCC 64677)		*Candida tropicalis* (ATCC 66029)	
	MIC (mg.L^{-1})	MFC (mg.L^{-1})	MIC (mg.L^{-1})	MFC (mg.L^{-1})	MIC (mg.L^{-1})	MFC (mg.L^{-1})
H2TTP	>10	>10	5	>10	5	5
[Mg(TTP)]	>10	>10	>10	>10	>10	>10
[Mg(TTP)(4-pypo)2] (**I**)	10	>10	2.5	5	5	5

The screening of the susceptibility of *M. canis* and *T. rubrum* clinical strains to H_2TTP, [Mg(TTP)] and **I** showed different results (Figure 13). The results of the screening indicate that [Mg(TTP)] and **I** have significant increasing inhibitory potentials for *both M. canis* and *T. rubrum*, with percentages of inhibition 74.07 % and 42% , respectively, and this with an initial concentration of 10 mg.mL^{-1}. In contrast, both [Mg(TTP)] and the free porphyrin exhibit weaker antidermatophytic effects, with percentage of inhibition values ranging from 11.11% to 16%. The negative control (10% DMSO)

showed no antidermatophytic activity. As a consequence of these promising results, the [Mg(TTP)] and [Mg(TTP)(4-pypo)$_2$]·2CH$_2$Cl$_2$ (**I**) complexes were selected for further experiment to determine the corresponding MIC.

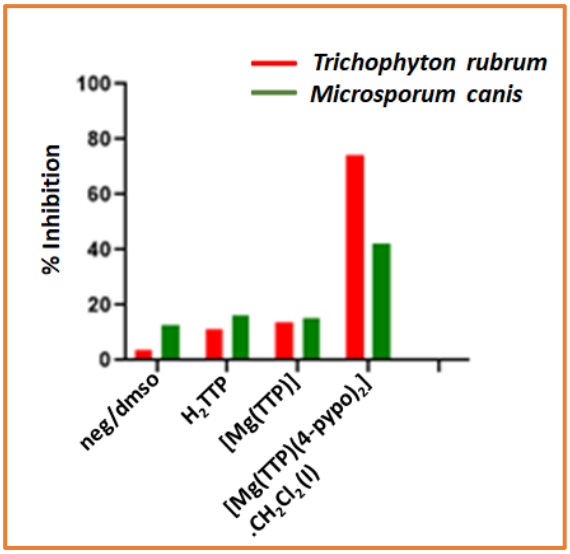

Fig. 13. Screening anti-dermatophyte activities of the different complexes

In an attempt to estimate MIC values, increasing concentrations of (1.25 mg.mL^{-1}, 2.5 mg.mL^{-1} and 5 mg.mL^{-1}) were tested. The percentages of inhibition of the tested strains by [Mg(TTP)] and [Mg(TTP)(4-pypo)$_2$]·2CH$_2$Cl$_2$ (**I**) are presented in Figure 14. We noticed that these two porphyrinic complexes inhibited the growth of dermatophytes mycelia in a dose-dependent manner. Indeed, each increase in porphyrin concentrations increased the inhibition of the fungal strains. At a concentration of 5 mg.mL^{-1} , [Mg(TTP)] and [Mg(TTP)(4-pypo)$_2$]·2CH$_2$Cl$_2$ (**I**) inhibited the mycelial growth of *M. canis* (71.42%), and *T. rubrum* (58.33%). The inhibition decreased over the days until it reached the percentage of 43.75% (*M. canis*) and 33.33% (*T. rubrum*) at the 5 mg concentration, 31.81% (*M. canis*) and 15.38% (*T. rubrum*) at the 2.5 mg.mL^{-1} concentration and 6.25 % (*M. canis*) and 5.56 % (*T. rubrum*) for the 1.25 mg.mL^{-1} concentration. According to these results, increasing the concentration of [Mg(TTP)] and [Mg(TTP)(4-pypo)$_2$]·2CH$_2$Cl$_2$ (**I**) remarkably increases the inhibition (Figure 14).

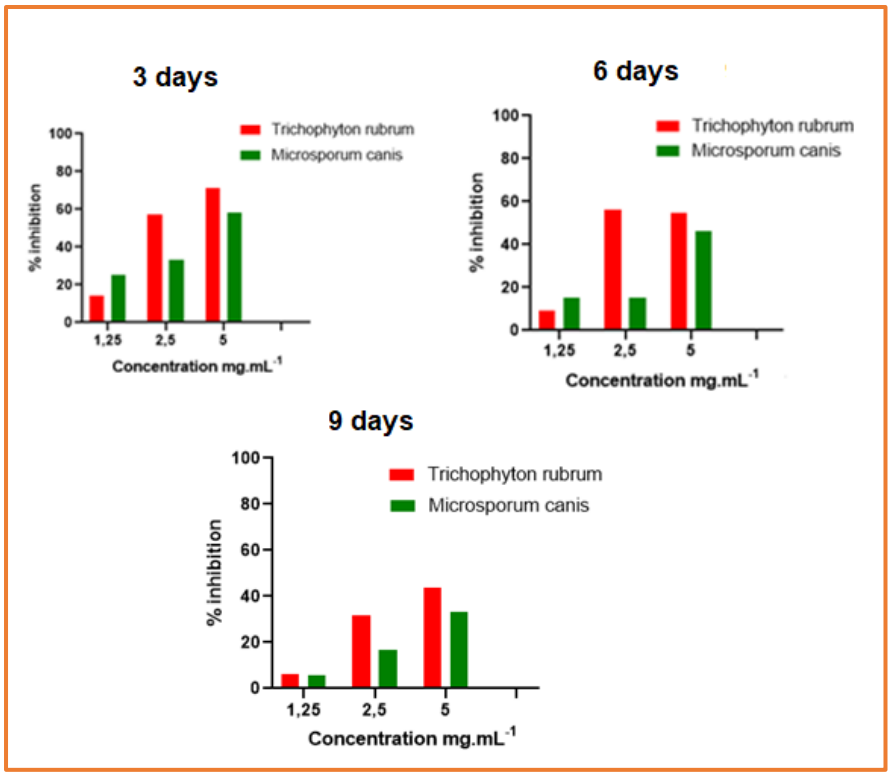

Fig 14. Anti-dermatophytes activity of [Mg(TTP)] and [Mg(TTP)(4-pypo)2]·2CH_2Cl_2 (**I**)

4. Conclusion

The preparation of a novel magnesium(II) porphyrin coordination compound [Mg(TTP)(4-pypo)$_2$] (**I**) with 4-pyrrolidinopyridine (4-pypo, $C_9H_{10}N_2O$) as axial ligand was successfully carried out. The single crystal X-ray molecular structure shows that **I** crystals in the triclinic crystal system with P-1 space group and in solid state this species presents two independent molecules [Mg1(TTP)(4-pypo)$_2$] and [Mg2(TTP)(4-pypo)$_2$] (1-2). The Hirshfeld surface analysis indicates that the crystal lattice of **I** is sustained by weak intermolecular interaction types C—H···C, C—H···Cg and C—H···Cl implicating molecules 1 and 2 and the dichloromethane solvent molecules. The H_2TTP free base porphyrin, the [Mg(TTP)] starting material and our Mg(II)-TTP-4-pypo (**I**) derivative were tested for their *in vitro* antifungal efficiency by microdilution method by determining the MIC and the MFC values. Complex **I** exhibits better activity against all the three strains of *Candida viz. C. albicans, C. glabrata* and *C. tropicalis* with MIC values in the range 2.5 to 10 $\mu g.mL^{-1}$. The results of the screening indicated that **I** have an important inhibitory potential for *both M. canis* and *T. rubrum*, with percentages of inhibition 74.07 % and 42%.

Declaration of Competing Interest

The authors declare that they have no known competing financial interests or personal relationships
that could have appeared to influence the work reported in this paper.

Supplementary materials

Supplementary material associated with this article can be found, in the online version, at doi:xxxxxxxxxxxxxxxxxxxxx.

4. References

[1] P. Biswal, S. Samser, P. Nayak, V. Chandrasekhar, K. Venkatasubbaiah, Cobalt(II) porphyrin-Mediated Selective Synthesis of 1,5-Diketones via an Interrupted-Borrowing Hydrogen Strategy Using Methanol as a C1 Source, J. Org. Chem. 86 (2021) 6744–6754, doi:10.1021/acs.joc.1c00476.

[2] D. J. Martin, J. M. Mayer, Oriented Electrostatic Effects on O_2 and CO_2 Reduction by a Polycationic Iron Porphyrin, J. Am. Chem. Soc. 143 (2021) 11423−11434, doi:10.1021/jacs.1c03132.

[3] K. Malecka, B. Kaur, D. A. Cristaldi, C. S. Chay, I. Mames, H. Radecka, J. Radecki, E. Stulz, Silver or gold? A comparison of nanoparticle modified electrochemical genosensors based on cobalt porphyrin-DNA, Bioelectrochemistry, 138, (2021 107723, doi:10.1016/j.bioelechem.2020.107723.

[4] W. C. Chan, H. M. Saad, K. S. Sim, V. S. Lee, C. Ang, K. Y. Yeong, K. W. Tan, A rhodamine based chemosensor for solvent dependent chromogenic sensing of cobalt(II) and copper(II) ions with good selectivity and sensitivity: Synthesis, filter paper test strip, DFT calculations and cytotoxicity, Spectrochim. Acta A Mol. Biomol. Spectrosc. 262 (2021) 120099, doi:10.1016/j.saa.2021.120099.

[5] D. Nishiori, B. L. Wadsworth, E. A. Reyes Cruz, N. P. Nguyen, L. K. Hensleigh, T. Karcher, G. F. Moore, Photoelectrochemistry of metalloporphyrin-modifed GaP semiconductors, Photosynth Res (2021), doi:10.1007/s11120-021-00834-2.

[6] M. Sabbaghan, M. Nadafan, V. J. Ahmadi, The effect of aromatic and non-aromatic ionic liquids on the optical nonlinearity responses of porphyrins, J. Mol. Liq. 348, (2022) 118398, doi:10.1016/j.molliq.2021.118398.

[7] C. R. Groom, I. J. Bruno, M. P. Lightfoot, S. C. Ward, The Cambridge Structural Database, Acta Cryst. B72 (2016) 171-179, doi:10.1107/S2052520616003954.

[8] K. Ezzayani, Z. Denden, Shabir Najmudin, C. Bonifácio, E. Saint-Aman, F. Loiseau, Habib Nasri, Exploring the Effects of Axial Pseudohalide Ligands on the Photophysical and Cyclic Voltammetry Properties and Molecular Structures of Mg(II) Tetraphenyl/porphyrin Complexes, Eur. J. Inorg. Chem. (2014) 5348–5361, doi:10.1002/ejic.201402546.

[9] N. Amiri, F. Ben Taheur, S. Chevreux, E. Wenger , G. Lemercier, H. Nasri, Synthesis, crystal structure and spectroscopic characterizations of porphyrin-based Mg(II) complexes e Potential application as antibacterial agent, Tetrahedron 73 (2017) 7011-7016, doi:10.1016/j.tet.2017.10.029.

[10] N. Amiri, M. Hajji, F. Ben Taheurc, S. Chevreux, T. Roisnele, G. Lemercier, Habib Nasri, Two novel magnesium(II) *meso*-tetraphenylporphyrin-based coordination complexes: Syntheses, combined experimental and theoretical structures elucidation, spectroscopy, photophysical properties and antibacterial activity, J. Solid State Chem. 258 (2018) 477–484, doi:10.1016/j.jssc.2017.11.018.

[11] A. Ben Khelifa, K. Ezzayani, M. Guergueb, F. Loiseau, E. Saint-Aman, H. Nasri, Synthesis, molecular structure, spectroscopic characterization and antibacterial activity of the pyrazine magnesium porphyrin coordination polymer, J. Mol. Struct. 1227 (2021) 129508, doi:10.1016/j.molstruc.2020.129508.

[12] T. Fradi, O. Noureddine, F. Ben Taheur, M. Guergueb, S. Nasri, N. Amiri, A. Almahri d, T. Roisnel, Vincent Guerineau, N. Issoui, H. Nasri, New DMAP meso -arylporphyrin Magnesium(II) complex. Spectroscopic, Cyclic voltammetry and X-ray molecular structure characterization. DFT, DOS and MEP calculations and Antioxidant and Antifungal activities, J. Mol. Struct. 1236 (2021) 130299, doi: 10.1016/j.molstruc.2021.130299.

[13] N. Amiri, F. Ben Taheur, S. Chevreux, C. M. Rodrigues , V. Dorcet, G. Lemercier, H. Nasri, Syntheses, crystal structures, photo-physical properties, antioxidant and antifungal activities of Mg(II) 4,4′-bipyridine and Mg(II) pyrazine complexes of the 5,10,15,20 tetrakis(4–bromophenyl)porphyrin, Inorg. Chim. Acta 525 (2021) 120466, doi:10.1016/j.ica.2021.120466.

[14] R. Calderone, N. Sun, F. Gay-Andrieu, W. Groutas, P. Weerawarna, S. Prasad, D. Alex, D. Li, Antifungal drug discovery: the process and outcomes, Future Microbiol. 9 (2014) 791-805, doi:10.2217/fmb.14.32.

[15] C. B. Machado, C. R. da Silva, F. D. Barroso, R. d. S. Campos, L. G. d. A. Valente Sá, F. B. S. Aires do Nascimento, B. C. Cavalcanti, H. V. Nobre Júnio, J. B. A. Neto, In vitro evaluation of anti-fungal activity of tropicamide against strains of Candida spp. resistant to fluconazole in

planktonic and biofilm form, Journal of Medical Mycology 31 (2021) 101080, doi:10.1016/j.mycmed.2020.101080.

[16] A. Hernández, S. Ruiz-Moyano, A. I. Galván, A. V. Merchán, F. P. Nevado, E. Aranda, M. J. Serradilla, M. d. G. Córdoba, A. Martín, Anti-fungal activity of phenolic sweet orange peel extract for controlling fungi responsible for post-harvest fruit decay, Fungal Biol. 125 (2021) 143-152, doi:10.1016/j.funbio.2020.05.005.

[17] A. Barbero-López, Antifungal Activity of Several Vegetable Origin Household Waste Extracts Against Wood-Decaying Fungi In Vitro. Waste Biomass Valor. 12 (2021) 1237–1241. doi:10.1007/s12649-020-01069-3.

[18] U. Singh, A. M. Malla, I. A. Bhat, A. A., Mohd, N. Bukhari, S. Bhat, S. Anayutullah, A. A. Hashmi, Synthesis, molecular docking and evaluation of antifungal activity of Ni(II),Co(II) and Cu(II) complexes of porphyrin core macromolecular ligand, Microbial Pathogenesis 93 (2016) 172-179, doi:10.1016/j.micpath.2016.02.011.

[19] S. Moghnie, A. Tovmasyan, J. Craik, I. Batinic-Haberle, L. Benov, Cationic amphiphilic Zn-porphyrin with high antifungal photodynamic potency Photochem. Photobiol. Sci. 16 (2017) 1709-1716, doi:10.1039/C7PP00143F.

[20] G. Karimipour. S. Kowkabi, A. Naghiha, New Aminoporphyrins Bearing Urea Derivative Substituents: Synthesis, Characterization, Antibacterial and Antifungal Activity, Braz. Arch. Biol. Technol. Braz. arch. biol. technol. 58 (2015) 431-442, doi:10.1590/S1516-8913201500024.

[21] R. L. Hill, M. Gouterman, A. Ulman, Tetraphenylporphyrin Molecules Containing Heteroatoms Other Than Nitrogen. Emission and Electronic Structure of Rings Containing Sulfur and Selenium, Inorg. Chem. 21 (1982) 1450-1455, doi:10.1021/ic00134a037.

[22] E. J. Shin, D. Kim, Substituent effect on the fluorescence quenching of various tetraphenylporphyrins by ruthenium tris(2,2-bipyridine) complex, J. Photochem. Photobiol. A 152 (2002) 25‑31. Doi:10.1016/S1010-6030(02)00189-2.

[23] J. Nishigaki, Y. Deguchi, Oxonol compound, silver halide photographic material and process for the synthesis of oxonol compound (1998), EP0819977A1

[24] A. D. Adler, F. R. Longo, J. D. Finarelli, J. Goldmacher, J. Assour, L. Korsakoff, " A simplified synthesis for *meso*-tetraphenylporphin", J. Org. Chem., 32, (1967) 476-476, doi:10.1021/jo01288a053.

[25] A. Ghosh, S. M. Mobin, R. Fröhlich, R. J. Butcher, D. K. Maity, M. Ravikanth, Inorg. Chem. 49 (2010) 8287–8297, doi:10.1021/ic1008522.

[26] SMART, SAINT, and SADABS, Bruker AXS Inc., (2008), Madison, WI, USA.

[27] A. Altomare, G. Cascarano, C. Giacovazzo, A. Guagliardi, M.C. Burla, G. Polidori, M. Camalli, SIRPOW.92 – A program for automatic solution of crystal structures by direct methods optimized for powder data, J. Appl. Crystallogr. 27 (1994) 435–436, doi:10.1107/S0 0218898940 0 0221.

[28] G.M. Sheldrick, Crystal structure refinement with SHELXL, Acta Cryst C71 (2015) 3–8, doi:10.1107/S2053229614024218.

[29] G.M. Sheldrick, Crystal structure refinement with SHELXL, Acta Cryst C71 (2015) 3–8, doi: 10.1107/S2053229614024218.

[30] P. McArdle, SORTX – A program for on-screen stick-model editing and autosorting of SHELX files for use on a PC, J. Appl. Crystallogr. 28 (1995) 65, doi:10.1107/S0021889894010642.

[31] L.J. Farrugia, J. Appl. Cryst. 30 (1997) 565, doi:10.1107/S0021889897003117.

[32] C. F. Macrae, I. J. Bruno, J. A. Chisholm, P. R. Edgington, P. McCabe, E. Pidcock, L. Rodriguez-Monge, R. Taylor, J. van de Streek, P.A. Wood, Mercury CSD 2.0 – New features for the visualization and investigation of crystal structures, J Appl Cryst. 41 (2008) 466–470, doi: 10.1107/S0021889807067908.

[33] S. Hrichi, R. Chaabane-Banaoues, D. Giuffrida, D. Mangraviti, Y. Oulad El Majdoub, F. Riganod, L. Mondello, H. Babba, Zine Mighri, F. Cacciola, Effect of seasonal variation on the chemical composition and antioxidant and antifungal activities of Convolvulus althaeoides L. leaf extracts, Arab. J. Chem. 13 (2020) 5651-5668, doi:10.1016/j.arabjc.2020.04.006.

[34] S. Nasri, I. Zahou, I. Turowska-Tyrk, T. Roisnel, F. Loiseau, E. Saint-Amant, H. Nasri, Synthesis, Electronic Spectroscopy, Cyclic Voltammetry, Photophysics, Electrical Properties and X-ray Molecular Structures of meso-{Tetrakis[4-(benzoyloxy)phenyl]porphyrinato}zinc(II) Complexes with Aza Ligands, Eur. J. Inorg. Chem. (2016), 5004–5019, doi:10.1002/ejic.201600575.

[35] Z. Denden, K. Ezzayani, E. Saint-Aman, F. Loiseau, S. Najmudin, C. Bonifácio, J. -C. Daran , H. Nasri, Insights on the UV/Vis, Fluorescence, and Cyclic Voltammetry Properties and the Molecular Structures of Zn(II) Tetraphenylporphyrin Complexes with Pseudohalide Axial Azido, Cyanato-N, Thiocyanato-N, and Cyanido Ligands, Eur. J. Inorg. Chem. (2015) 2596–2610, doi:10.1002/ejic.201403214.

[36] C. Mchiri, H. Nasri, C. Frochot, S. Acherar, Distorted five-coordinate square pyramidal geometry of a cadmium(II) complex containing a 2-methylimidazole ligand: Crystal structure and axial ligand effect on spectroscopic properties, Polyhedron 173 (2019) 114107, doi:10.1016/j.poly.2019.114107.

[37] U. Tripathy, D. Kowalska, X. Liu, S. Velate, R. P. Steer, Photophysics of Soret-Excited Tetrapyrroles in Solution. I. Metalloporphyrins: MgTPP, ZnTPP, and CdTPP J. Phys. Chem. A 112 (2008) 5824-5833, doi:10.1021/jp801395h.

[38] J. W. Owens, R. Smith, R. Robinson, M. Robins, Photophysical properties of porphyrins, phthalocyanines, and benzochlorins, Inorg. Chim. Acta 279 (1998) 226-231, doi:10.1016/S0020-1693(98)00137-6.

[39] M. Guergueb, S. Nasri, J. Brahmi, F. Loiseau, F. Molton, T. Roisnel, V. Guerineau, I. Turowska-Tyrk, K. Aouadi, H. Nasri, Effect of the coordination of π-acceptor 4-cyanopyridine ligand on the structural and electronic properties of meso - tetra(para -methoxy) and meso -tetra(para -chlorophenyl) porphyrin cobalt(II) coordination compounds. Application in the catalytic degradation of methylene blue dye, RSC Adv 10 (2020) 6900–6918, doi:10.1039/C9RA08504A.

[40] A. Ghosh, S. M. Mobin, R. Fröhlich, R. J. Butcher, D. K. Maity, M. Ravikanth, Effect of Five Membered Versus Six Membered *Meso*-Substituents on Structure and Electronic Properties of Mg(II) Porphyrins: A Combined Experimental and Theoretical Study, Inorg. Chem. 49 (2010) 8287–8297, doi:10.1021/ic1008522.

[41] K. Ezzayani, A. Ben Khelifa, F. Ben Taheur, M. Guergueb, A. Mansour, J. -C. Daran, H. Nasri, Effect of the coordination of π-acceptor 4-cyanopyridine ligand on the structural and electronic properties of meso-tetra(para-methoxy) and meso-tetra(para-chlorophenyl) porphyrin cobalt(II) coordination compounds. Application in the catalytic degradation of methylene blue dye, Inorg. Chim. Acta 514 (2021) 119960, doi:10.1016/j.ica.2020.119960.

[42] K. Ezzayani, A. Ben Khelifa, E. Saint-Aman, F. Loiseau, H. Nasri, Complex of hexamethylenetetramine with magnesium-tetraphenylporphyrin: Synthesis, structure, spectroscopic characterizations and electrochemical properties, J. Mol. Struct. 1137 (2017) 412-418, doi:10.1016/j.molstruc.2017.02.054.

[43] L.-Yi Shu, H. Sun, Q. Wang, S. Tun, Progress in Binding Affinities of Metal Porphyrins to Heterocycles and DNA, Chinese Journal of Organic Chemistry 11 (2009) 1700-1707.

[44] D. J. Quimby, F. R. Longo, Luminescence studies on several tetraarylporphins and their zinc derivatives, J. Am. Chem. Soc. 97, (1975) 5111–5117, doi:10.1021/ja00851a015.

[45] K. Oberda, I. Deperasinska, Y. P. Nizhnik, A. Szemik-Hojniak, A novel complex of zinc tetraphenylporphyrin with two dioxane molecules in a rare attachment. Crystal structure, spectroscopy and theoretical calculations, Polyhedron 51 (2013) 61-69, doi:10.1016/j.poly.2012.12.014.

[46] C. Mchiri, A. Ouakouak, S. Nasri, A. Jedidi, I. Turowska-Tyrk, S. Acherar, C. Frochot, T. Roisnel, H. Nasri, DABCO cadmium(II) tetrakis(4-metoxyphenyl)porphyrin complex – Structure, photophysical properties, and adsorpion removal of methylene blue dye, Inorg. Chim. Acta, 515 (2021) 120046, doi:10.1016/j.ica.2020.120046.

[47] C. Mchiri, B. Gassoumi, S. Acherar, M.A.M. Sh. El-Sharief, H. Nasri, Synthesis, X-ray molecular structure and QTAIM and NCI-RDG theoretic studies of a new cadmium (II) (4-4' diaminodiphenylmethane)(*meso*-arylporphyrin) coordination compound, Inorg. Chem. Commun. 133 (2021) 108924, doi:10.1016/j.inoche.2021.108924.

[48] C. Mchiri, S. Dhifaoui, k. Ezzayani, M. Guergueb, T. Roisnel, F. Loiseauc, H. Nasri, Insights into the new cadmium(II) metalloporphyrin: Synthesis, X-ray crystal structure, Hirshfeld surface analysis, photophysical and cyclic voltammetry characterization of the (morpholine){(*meso*-tetra(para-chloro-phenyl)porphyrinato}cadmium(II), Polyhedron 171 (2019) 10-19, doi:10.1016/j.poly.2019.06.055.

[49] V. McKee, O. C. Choon, G. A. Rodley, X-ray crystal and molecular structures of related octahedral magnesium tetraphenylporphyrin complexes, Inorg. Chem. 23 (1984) 4242–4248, doi: 10.1021/ic00193a029.

[50] M. P. Byrn, C. J. Curtis, Y. Hsiou, S. I. Khan, P. A. Sawin, S. K. Tendick, A. Terzis, C. E. Strouse, Porphyrin sponges: conservative of host structure in over 200 porphyrin-based lattice clathrates, J. Am. Chem. Soc. 115 (1993) 9480–9497, doi:10.1021/ja0 0 074a013.

[51] C. C. Ong, V. McKee, G. A. Rodley, The crystal and molecular structure of a monohydrated dipicoline magnesium tetraphenylporphyrin complex, Inorg. Chim. Acta 123 (1986) L11–L14, doi: 10.1016/S0020-1693(00)84300-5.

[52] K. Ezzayani, M. S. Belkhiria, S. Najmudin, C. Bonifácioc, H. Nasri, Aqua-(4-cyano-pyridine-κN (4))(5,10,15,20-tetra-phenyl-porphyrinato-κ(4) N)magnesium, Acta Crystallogr Sect E Struct Rep Online 69 (2012) m17–m18, doi:10.1107/s1600536 81204 9434.

[53] M. J. Turner, J. J. McKinnon, S. K. Wolff, D. J. Grimwood, P. R. Spackman, D. Jayatilaka, M. A. Spackman, CrystalExplorer17; University of Western Australia, 2017.